NUMERICAL SIMULATION AND EXPERIMENTAL VALIDATION OF TWIN WIRE ARC ADDITIVE MANUFACTURING OF CoCrNi-MEDIUM ENTROPY ALLOY

MTech Thesis

By

Rajshree Singh

(2202103027)

DISCIPLINE OF MECHANICAL ENGINEERING

INDIAN INSTITUTE OF TECHNOLOGY INDORE

JUNE 2024

NUMERICAL SIMULATION AND EXPERIMENTAL VALIDATION OF TWIN WIRE ARC ADDITIVE MANUFACTURING OF CoCrNi- MEDIUM ENTROPY ALLOY

A THESIS

Submitted in partial fulfillment of the

requirements for the award of the degree

of

Master of Technology

by

RAJSHREE SINGH

DISCIPLINE OF MECHANICAL ENGINEERING

INDIAN INSTITUTE OF TECHNOLOGY INDORE

JUNE 2024

INDIAN INSTITUTE OF TECHNOLOGY INDORE

CANDIDATE'S DECLARATION

I hereby certify that the work which is being presented in the thesis entitled **NUMERICAL SIMULATION AND EXPERIMENTAL VALIDATION OF TWIN WIRE ARC ADDITIVE MANUFACTURING OF CoCrNi-MEA** in the partial fulfilment of the requirements for the award of the degree of **MASTER OF TECHNOLOGY** and submitted in the **DISCIPLINE OF MECHANICAL ENGINEERING, Indian Institute of Technology Indore**, is an authentic record of my own work carried out during the time period from May 2023 to June 2024 under the supervision of **Dr. Dan Sathiaraj**, Associate Professor, Department of Mechanical Engineering, Indian Institute of Technology, Indore.

The matter presented in this thesis has not been submitted by me for the award of any other degree of this or any other institute.

Rajshree Singh 13/06/24

Signature of the student with date

RAJSHREE SINGH

This is to certify that the above statement made by the candidate is correct to the best of my/our knowledge.

13/06/24

Signature of the Supervisor

Dr. Dan Sathiaraj

---

has successfully given his/her M.Tech. Oral Examination held on **30/05/2024**.

13/06/24

Signature(s) of Supervisor(s) of M.Tech. thesis

Convener, DPGC 13/06/24

ACKNOWLEDGEMENT

I extend my heartfelt gratitude to Dr. Dan Sathiaraj, my supervisor, whose invaluable expertise and inspiration were pivotal to this work. I deeply appreciate Miss Poonam Deshmukh, Rajnish Prakash Modanwal, and Mr. Rajendra Goud for their unwavering support and guidance. My sincere thanks to my labmates, Mr. Vipin Goyal, Mr. Harsh Vardhan Singh, Mr. Rishabh Kumar, and Mr. Prasanna Bairagi, for their camaraderie and support. The collaborative spirit and assistance from my lab have been instrumental. I also extend my gratitude to the evaluation committees, faculty, and IIT Indore for their valuable input and providing me with this opportunity.

Rajshree Singh
13/06/24

With Regards

Rajshree Singh

DEDICATION

This thesis is dedicated to my Parents and Prakhar Doshi, whose boundless support and encouragement have been my pillars of strength throughout this journey.

ABSTRACT

This research investigates the design and development of CoCrNi medium entropy alloy (MEA) using Twin Wire Arc Additive Manufacturing (TWAAM), integrating both experimental fabrication and numerical simulation. The CoCrNi MEA, known for its outstanding properties at cryogenic and high temperatures, was fabricated using a GMAW-based TWAAM setup with optimized parameters. Two structures were created: a wall (108 mm x 10 mm x 24 mm) and a plate with 30% bead overlap (108 mm x 24 mm x 6 mm). A 3D transient thermos-mechanical model was developed using Abaqus and Goldak's heat source model, providing insights into temperature distribution and residual stress formation. Numerical results indicated that preheating enhanced layer fusion and reduced residual stresses, which were consistent with experimental observations. This integrated approach highlights the potential of TWAAM for producing high-quality CoCrNi MEA components, underscoring the significance of optimized parameters and effective thermal management. The numerical model serves as a predictive tool for temperature and stress distributions, aiding future process optimizations. This study addresses a critical gap in the additive manufacturing of MEAs with TWAAM.

LIST OF FIGURES

LIST OF TABLES

ABBREVIATIONS

AM	Additive manufacturing
WAAM	Wire arc additive manufacturing
TWAAM	Twin Wire arc additive manufacturing
MEA	Medium Entropy Alloy
XRD	X-ray Diffraction
MIG	Metal inert gas

Table of Contents

Chapter 1: INTRODUCTION

1.1 Additive Manufacturing:

Additive manufacturing (AM) is the advanced manufacturing technique that forms the final component by stacking layers of raw materials one upon another.

A basic AM system consists of a combination of a motion system, heat source and feedstock.

1.1.1 Classification of AM processes:

The below classification of AM process (shown in Figure 1) is based on the different methods or techniques used for adding layers of material to create a 3D object:

Material extrusion: Also known as Fused Deposition Modelling (FDM), this additive manufacturing process involves the deposition of melted material through a nozzle or extruder. Commonly used materials include thermoplastics, waxes, and metals.

Vat photopolymerization: This process uses a vat of liquid photopolymer resin that is cured layer by layer using a UV light. It is commonly used for creating highly detailed objects, such as dental and jewellery models.

Binder jetting: This process involves the deposition of a binder onto a powder bed layer by layer. The binder acts as an adhesive, bonding the powder together to create a solid object. Binder jetting is commonly used for creating metal, ceramic, and sand moulds for casting.

Powder bed fusion: This type of additive manufacturing involves melting or sintering powdered material, such as metal, ceramic, or polymer, layer by layer using a laser or electron beam. Examples include selective laser sintering (SLS), direct metal laser sintering (DMLS), and electron beam melting (EBM).

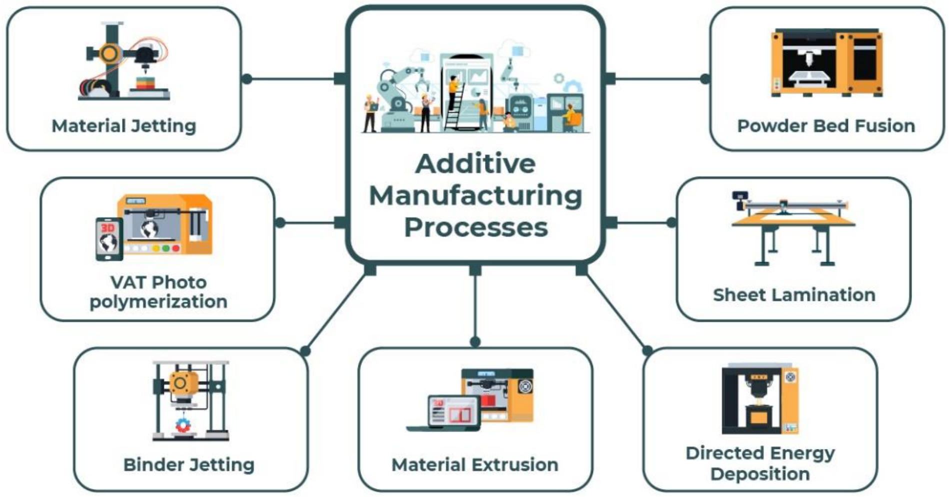

Fig.1. Classification of AM processes [1]

Directed energy deposition: This process involves the deposition of melted material through a nozzle onto a substrate. It is commonly used for repairing or adding material to an existing part or for creating new parts from scratch. Examples include laser engineered net shaping (LENS) and direct energy deposition (DED).

Material Jetting: This type of additive manufacturing uses an inkjet printer to deposit droplets of material layer by layer. It is commonly used for printing multi-material objects, such as those with varying colors or densities. Examples include polyjet and binder jetting.

1.2 Wire Arc Additive Manufacturing (WAAM):

Wire arc additive manufacturing (WAAM) is a metal additive manufacturing process that uses an electric arc to melt a wire feedstock and deposit it layer by layer to build up a 3D object. The wire is fed continuously into the arc, which melts the wire into a melt pool and deposits it onto the workpiece.

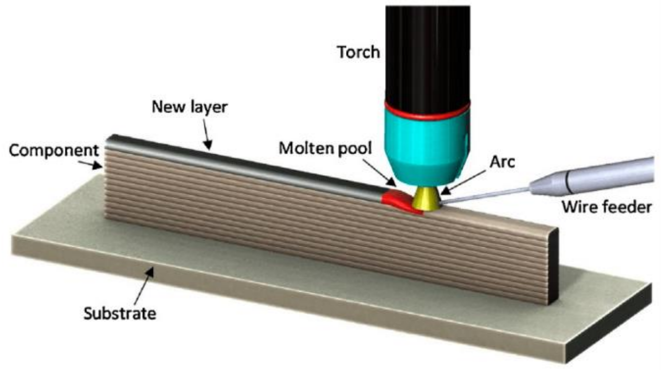

Fig.2. Schematic of WAAM [2]

Depending upon the working principle of arc formation WAAM can be classified as MIG, TIG or plasma arc type WAAM.

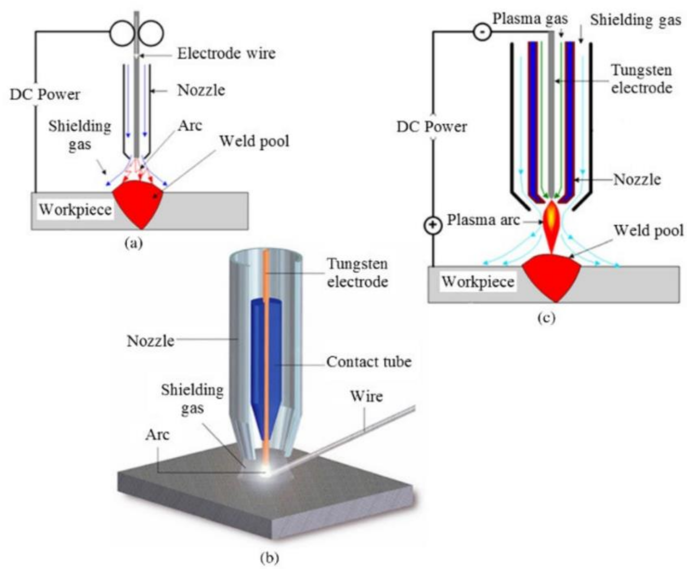

Fig.3. Wire Arc Additive Manufacturing. Principle of WAAM with: (a) MIG; (b) TIG; (c) PA [2]

1.2.1 Advantages of WAAM process:

Using the WAAM technique, 3D components may be produced with more freedom. There is no need for external machine equipment, dies, or casting molds [11]. With a rapid deposition rate and minimal material waste, this WAAM method has a very high degree of feed material utilization. When manufacturing complicated parts or components, less material waste might result in lower potential costs and shorter lead times[3]. The Layer-by-layer deposition characteristics is used to create complex parts and preforms of medium and large sizes that are close to net shapes. Moreover, the generated part is accurate and has a superior surface polish.

1.2.2 Disadvantages of WAAM:

The heat generated is relatively high compared to other additive manufacturing processes, generating residual strains and distortions in the finished component [4]. Also, the complex part production can be considered to have a lower level of surface polish. In some circumstances, the operator's competence and ongoing observation are necessary for a successful build-up of layers; otherwise, cracks may emerge. Moreover, to get rid of splatter and extra material on the substrate, post finishing processes are carried out.

1.3 Twin Wire Arc Additive Manufacturing:

Lack of commercially available alloy wires poses challenges in the preparation and composition design of certain alloys via WAAM. For additively manufacturing multi component alloy we can employ multiple wires instead of one single wire like WAAM.

To address the challenge of availability of alloy wires in manufacturing multiple principal component alloy, two feed wires of any can be used in the T-WAAM technology, depending on the user requirement. [5] Separate power sources are supplied to each wire feeder so that they can independently adjust the process settings. Consequently, it is possible to acquire the various alloy compositions.

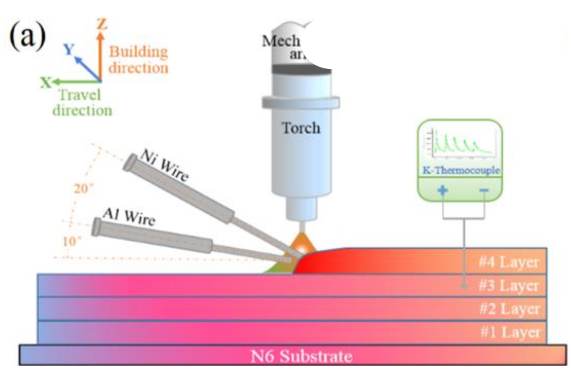

Fig.4 Schematic of T-WAAM [6]

1.4 CoCrNi and its applications:

The CoCrNi Medium Entropy Alloy is a highly studied subset of the Cantor alloy because of its excellent properties at elevated and cryogenic temperatures. CoCrFeMnNi HEA and its derivative alloys have been the subject of extensive research, with particular emphasis on mechanical characteristics and microstructure evolution. According to the studies, the CoCrNi MEA outperforms the CoCrFeMnNi HEA. The studies have concluded that the CoCrNi MEA possesses superior low-cycle fatigue strength and cryogenic and high-temperature strength. compared to CoCrFeMnNi HE.[7]

Because of its exceptional qualities, including high strength, high temperature oxidation resistance, and corrosion resistance, MEA is extensively employed in the aerospace industry. [8]

Fig. 5. Specific applications of MEA in aerospace: engines, combustion chambers, turbine blades, jet tubes and fuselage support. [8]

For fabrication of HEAs and MEAs Conventional casting and spark plasma sintering have been the most widely used methods. Such Conventional methods requires a lot of post processing in order to achieve a defect-free homogenous microstructure.

Additive manufacturing (AM) techniques can be opted for fabricating novel materials with complex shapes.

1.5 Residual stresses in metal additive manufacturing:

Metal additive manufacturing (MAM) offers versatile applications in aerospace, medical, and energy sectors, but its complex process induces significant residual stresses, impacting dimensional stability and mechanical properties.

The MAM process's intense thermal, mechanical, and metallurgical coupling causes the produced samples to have significant residual stresses. The dimensional stability, resistance to corrosion, resistance to crack formation, and mechanical properties of MAM samples are all significantly impacted by residual stress.

Consequently, residual stress can be considered a critical factor in cost management, improving the effectiveness and quality of the product.

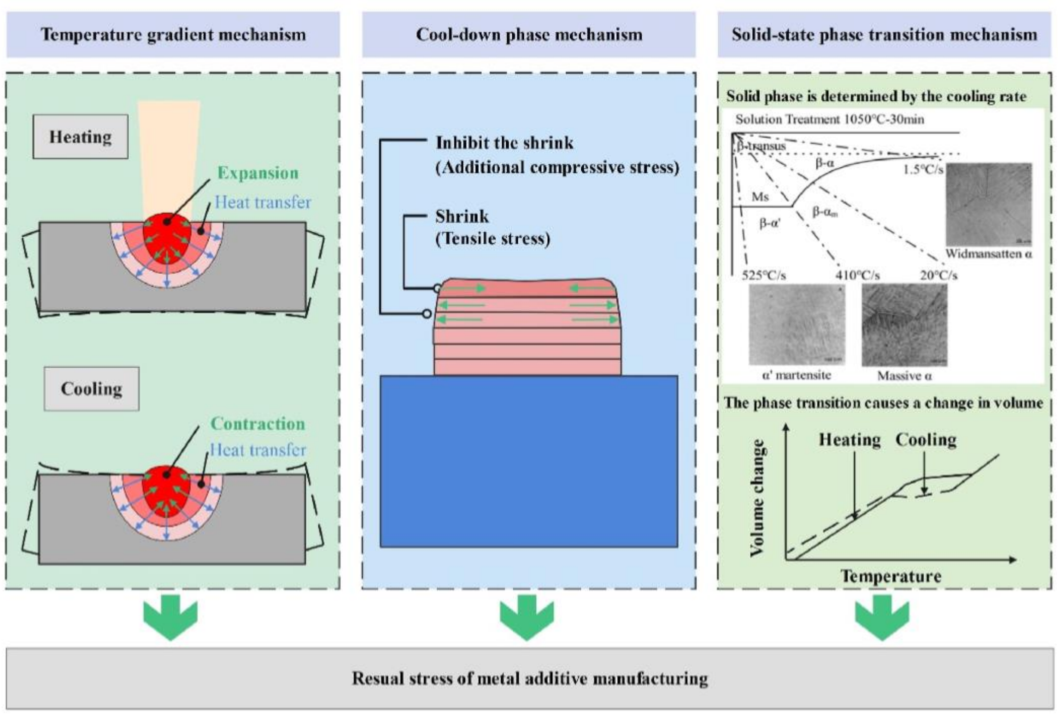

Fig. 6. Mechanisms of residual stress formation in MAM[9]

Enhancing the process optimization of MAM requires a robust and validated residual stress and deformation prediction model. In addition to saving time and cost as compared to experimental methods, it can also help researchers gain a better understanding of the evolution and parameter dependency of residual stress in the MAM process[9].

1.6 Numerical simulation of TWAAM process:

The complex thermo-mechanical phenomena of additive manufacturing are influenced by several process variables, including as scanning speed, dwell time, feed rate, voltage, current, and materials. Each component, material, and AM process variation requires a different approach to trial and error when producing and certifying additive manufacturing (AM) parts. To enhance the design of AM components, effective and reliable numerical tools that can accurately represent the AM process are required[10].

Building numerical models that can accurately predict defect development or solidification structure under any given process parameter is therefore crucial for additive manufacturing (AM) technologies. Instead of using experimental approaches, numerical simulations can accurately represent the melting pool, which is required for predicting residual stresses, distortions, and grain structure and texture.

Chapter 2: LITERATURE REVIEW

Fei Weng, et at. [11]. Fabricated CoCrNi (MEA) using laser-aided additive manufacturing (LAAM). The alloy demonstrated impressive mechanical properties: an ultimate tensile strength (UTS) of 873.5 MPa, a yield strength (YS) of 620.5 MPa, and an elongation after fracture (δF) of 44.8%, all without any post heat treatment. Lattice friction stress, boundary strengthening, and dislocation strengthening are the main causes of the high YS. Steady work hardening and delayed fracture are facilitated by deformation twinning that occurs during tensile deformation. LAAM proves to be an effective method for fabricating high-performance alloys like CoCrNi MEA.

Deshmukh, Poonam S., et al. [7] CoCrNi (MEA) was fabricated by LDED using High purity(>99%) powders of pure Co, Cr, and Ni . Along SD and BD, the σy values are 386 ± 8.45 MPa and 370.62 ± 10.40 MPa, respectively. Along the SD and BD directions, percentage elongation (δL) was observed to be 43.02 ± 8.32% and 64.90 ± 7.54 %, respectively. According to this study, LDED is feasible technique to fabricate CoCrNi(MEA).

Kyung-Hwan Jung et al. [12] In this work, the cryogenic mechanical characteristics and microstructure of CrCoNi medium entropy alloy (MEA) produced by hot isostatic pressing (HIP) and selective laser melting (SLM) were investigated.Optimal SLM processing parameters yielded a high relative density of 99.97% and micro-hardness. At 150 K, the CrCoNi MEA demonstrated superior strength and ductility. HIP treatment further enhanced ductility while maintaining strength. TEM analysis indicated that the synergistic effects of dislocations and twinning contribute to exceptional cryogenic performance, showcasing the potential of SLM and HIP for high-performance cryogenic applications

Shu-guang Chen[9] The review comprehensively addresses the critical role of residual stress in metal additive manufacturing (MAM), a cutting-edge technology with significant potential in various industries such as aerospace, medical, and energy. Residual stress, stemming from the intricate thermal, mechanical, and metallurgical interactions during MAM processes, profoundly influences the dimensional stability, corrosion resistance, and mechanical properties of manufactured components. The study systematically examines key aspects including formation mechanisms, detection techniques, parameter dependencies, prediction methodologies, and control strategies pertaining to residual stress in MAM. Notably, it emphasizes the importance of achieving accurate prediction and effective control of residual stress to optimize the performance and reliability of MAM-produced parts. Additionally, the review advocates for the development of flexible process strategies and closed-loop approaches to mitigate residual stress challenges and enhance the overall efficiency and effectiveness of MAM processes.

S. W. Williams, et al. [13] Paper describes Wire + Arc Additive Manufacturing that allows the deposition of large metal components with benefits like higher deposition rates, cost-efficiency, and structural integrity. It also suggests strategies for managing issues like residual stress and defects.

M Saadatmand et al [14] investigated the thermal behavior in the WAAM process of a carbon steel (ASTM A36) four-layer wall using a 3D model in ABAQUS. Significant findings shows that the peak temperature rises with the number of deposited layers (from 2518°C to 2640°C) while the average cooling rate decreases (from 123°C/s to 115°C/s). Substrate preheating elevates the peak temperature of the first layer (from 2518°C to 2600°C) and reduces its cooling rate (from 123°C/s to 118°C/s). Additionally, travel speed significantly affects the thermal behavior and metallurgical bonding of the layers, emphasizing its critical role in the WAAM process.

M. A. Somashekara et al. [15] study showed that TWAAM based on gas metal arc welding has the ability to create functionally gradient objects with different mechanical properties, such as hardness, by using different filler wires (ER70S-6 and ER110S-G) and controlling their proportions. Key experiments analyzed the impact of process parameters on bead geometry and identified optimal operating ranges. It also found that torch direction does not affect weld hardness, but overlapping beads result in lower hardness compared to single beads due to reheating and partial remelting. A proof of concept for twin-wire weld deposition is presented in the paper, and experiments were conducted to determine how the weld-deposition process parameter affects bead geometry. The operational range of various filler wire combinations was found, along with the range of process parameters for each combination.

R. Pramod et al [16] When gas metal arc welding was used to create a 347 stainless steel (SS347) plate utilizing WAAM technology, the resulting tensile characteristics demonstrated increased strength in comparison to wrought SS347.Microhardness ranged from 265 to 226 HV 0.5, and ferrite measurements were between 2.2 to 5.1 FN. Strong <001> texture in the building direction (BD) with well-aligned equiaxed and columnar dendrites and a reduced fraction of niobium carbide (NbC) was revealed by electron backscatter diffraction (EBSD) analysis.A 3D finite element model using the Goldak heat source predicted temperature distribution, residual stress, and plastic strain. Additionally, the study noted excellent inter-layer metallurgical bonding and no defects in bend tests.

Goldak et al. [17] presents a new mathematical model for welding heat sources based on a Gaussian distribution of power density in space. The model proposes a double ellipsoidal geometry that can easily change the size and shape of the heat source to model both shallow and deep penetration welding processes. The model is compared to previous models and experimental results, showing excellent agreement. The article emphasizes the importance of accurate modeling of the weld heat source in predicting residual stress, distortion, and strength of welded structures. In conclusion, the double ellipsoidal model is found to be more accurate than conventional analytical solutions and can be adapted to different welding geometries. The article provides technical details and equations for the model and includes verification of the model through analysis of two different welding situations. The paper highlights the significance of accurate modeling of the weld heat source in predicting the behavior of welded structures.

Mishra, Rajnish, et al.[18] The work uses experimental and finite element simulations (FES) to examine residual stresses and deformation that occur during weld bead deposition.The residual stresses and distortions discovered in the experiment correlate well with the results of the FE models. The regulation of thermal stresses during multi-layer deposition is the main emphasis of this study. To assess residual stresses and distortion, experimental techniques as well as finite element simulations (FES) were used. The element birth approach was applied to two welding pass with 32% lateral overlap using ABAQUS. The temperature gradient-driven residual stresses and distortion were measured using a passive coupled thermo-mechanical model that was monitored online using thermocouples. The correctness of the numerical model was confirmed by measurements of residual stresses and distortion made using a coordinate measuring machine (CMM) and X-ray diffraction (XRD), which showed good agreement with the findings of the FES.

Jiamin Sun[19] This study performed numerical simulations and experiments to analyse residual stress (RS) in wire and arc additive manufacturing (WAAM) components made of aluminium alloys. Results indicated that beam height significantly affects longitudinal RS in both the substrate and beam, with a transition from tensile to compressive RS on the top layer if the beam height exceeds 20 mm. Transverse RS in the substrate is influenced by beam height, while in the beam it remains relatively unaffected. The substrate's restraint conditions impact longitudinal RS in the beam but have minimal effect on transverse RS. These findings offer insights into managing RS in WAAM components.

Rajnish Mishra[20] This paper explores the issues of residual stress and distortion in Inconel 625 parts produced by wire arc additive manufacturing (WAAM) with cold metal transfer (CMT). Utilizing Finite Element (FE) thermo-mechanical simulations in Abaqus software, residual stress evolution was analyzed, revealing a reduction of 50% in residual stresses upon clamp removal. Process parameter optimization yielded defect-free additive bead layers, achieving an optimal heat input per unit length (Q) of 200.97 J/mm. Key conclusions include successful validation of predicted thermal histories against experimental thermocouple data and characterization of residual stress distributions within deposited beads and substrate material. These insights offer valuable guidance for enhancing the accuracy and reliability of Inconel 625 components in additive manufacturing.

Chapter 3: MOTIVATION, OBJECTIVES AND RESEARCH METHODOLOGY

3.1 Motivation

CoCrNi Medium Entropy Alloy (MEA), a variant of the Cantor alloy, stands out for its remarkable properties, especially in extreme conditions like cryogenic and high temperatures. Traditional methods such as casting and spark plasma sintering have been extensively used to create High Entropy Alloys (HEAs) and MEAs. However, these methods often require extensive post-processing to achieve the desired microstructure quality and homogeneity.

Additive Manufacturing (AM) offers an exciting avenue for fabricating MEAs. Unlike conventional techniques, AM allows for the creation of intricate designs and complex shapes directly from digital models. This technology has the potential to streamline the fabrication process, reduce post-processing steps, and ultimately, produce defect-free components.

Based on the literature reviews, there is a significant gap in research regarding the fabrication of CoCrNi (MEA) using Twin Wire Arc Additive Manufacturing (TWAAM) and the numerical simulation of this process. While several studies have explored the fabrication of MEA using Laser based additive manufacturing, fabrication of CoCrNi MEA fabrication via TWAAM has not been reported yet. Additionally, because there are so many factors involved in TWAAM processing, optimization is a crucial and time-consuming experimental job, necessitating the necessity for an appropriate numerical simulation of the procedure. As a result, the process' numerical simulation is also carried out.

This research aims to fill this gap by investigating the residual stresses of CoCrNi MEA fabricated through TWAAM, providing valuable insights for optimizing the manufacturing process and enhancing the quality of CoCrNi MEA components.

The aim is to fabricate CoCrNi wall and plate structures using optimized parameters, conduct experimental investigation of residual stress via Residual XRD, develop a numerical simulation model of the TWAAM process, and validate the results obtained from numerical simulations with experiments.

3.2Objectives

- Fabrication of CoCrNi wall structure at optimized parameters
- Fabrication of CoCrNi Plate(30% bead overload) structure at optimized parameters
- Investigation of Residual stress via XRD
- Development of a Numerical simulation model of TWAAM process
- Validation of the results obtained from numerical simulation.

3.3Methodology of Research

Experimental Fabrication

The fabrication of CoCrNi medium entropy alloy (MEA) was carried out using a gas metal arc welding (GMAW) based Twin Wire Arc Additive Manufacturing (TWAAM) setup, specifically the Reliable MIG 400HD model. Optimized parameters were determined to ensure quality deposition.Two types of structures were fabricated—a wall structure (108 * 10 * 24 mm) and a plate structure with 30% bead overlap (108 * 24 *6 mm) on a mild steel substrate. The deposition process was controlled using MACH 3 software, which enabled precise manipulation of the torch path and speed, ensuring consistent bead geometry and optimal layer adhesion. Post-fabrication, the residual stresses in the deposited structures were measured using X-ray diffraction (XRD). Samples for XRD analysis were cut into 20 x 20 x 5.5 mm for the substrate and 20 x 20 x 10 mm for the deposition, and the residual stresses were calculated from the d-spacing variations at different tilt angles (ψ) according to Bragg's law.

Numerical Simulation

A numerical simulation model was developed using Abaqus software to understand the thermal and mechanical behavior during the TWAAM process. The thermal analysis employed Goldak's double ellipsoidal heat source model, implemented via a Fortran-written Dflux subroutine. Parameters for the heat source model were derived from the geometry of the deposited beads. The simulation involved layer-by-layer activation and deactivation, with the interactions and loads managed through Python scripts integrated into Abaqus. The temperature distribution obtained from the thermal analysis was then used as a predefined field input for the subsequent mechanical analysis, which assessed residual stresses using elastic-plastic material behavior

Chapter 4: EXPERIMENTAL WORK

4.1 Experimental Setup:

Twin wire welding based additive manufacturing is a unique method that uses gas metal arc welding (GMAW). The experimental setup schematic shown in fig.7 represents the indigenously developed TWAAM setup.

This indigenously developed TWAAM setup integrates five key units:

(i) A 3-axis CNC worktable that mounts the base plate, with its controller programmed in G and M codes via a dedicated computer. The motion of CNC system is controlled through a software in computer system ("MACH3")

(ii) A welding machine setup (Make and Model: Reliable MIG 400HD), an inverter converts the DC voltage which rectified from input 50/60 Hz AC and gives output current and voltage in the range of 20 to 400 A and 12 to 34V. The efficiency of the machine can reach up to 85%, and save energy by 30% compared with the traditional machine.

(iii) A feeding system that implied feedstock material and wire feeder (Model: CS.401Y)

(iv) A system that supplies shielding gas (argon) to the weld pool and deposition, and

(v) The setup on CNC for wire feed nozzles were positioned at 60° relative to the substrate surface with a horizontal angle of 60° between the twin-wire feed nozzles.

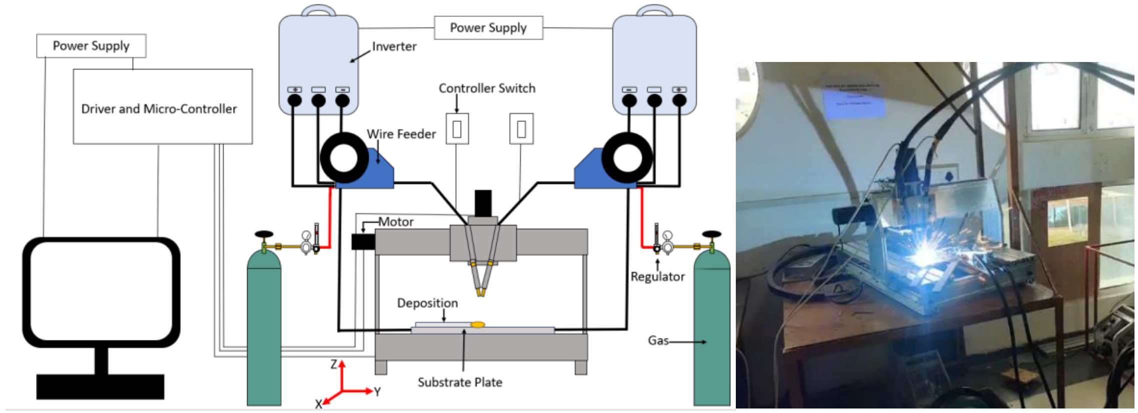

(a) (b)

Fig. 7. (a) Schematic of MIG based T-WAAM setup (b) Deposition in MIG based T-WAAM

4.2 Experimental methodology:

For the TWAAM of CoCrNi, a gas metal arc welding (GMAW) based setup is used (Make and Model: Reliable MIG 400HD). The setup diagrams are displayed in Fig12. In order to create an arc between the metals and substrate, a direct current (DC) power source is used in this process to provide current and voltage between 20 and 400 A and 12 and 35 V. In order to fuse the incoming feedstock metal with the base plate or the previously deposited layer, this arc acts as a heat source to melt it. Coaxially supplied inert gas(argon)is used in the T-WAAM process to protect the molten deposition from the external environment. In order to fabricate a wall, build structure and plate structure (30% overlap beads with 3 passes) MACH 3 software is used which helps in coding the pattern of deposition and also controlling the torch speed.

4.3 Material used:

In the twin wire weld deposition system, the two filler wires are kept firmly apart inside a single torch, and the process parameters may be adjusted independently for each of them.

In both weld deposition patterns in this investigation, Ni-Cr alloy and Co filler wires with a diameter of 1.2 mm were employed.

A mild steel substrate plate of 150*70*5.5 dimensions is used.

Fig.8. Two filler wires in single torch setup

4.4 Process parameters used for the experiment:

Wire arc additive manufacturing (WAAM) usually requires a lot of parameter control. The wire feed speed (m/min), torch travel speed (mm/s), voltage, current, flow rate of inert gas, etc. are typical process characteristics. Controlling each of these characteristics is necessary to ensure deposition that is smooth, continuous, and free of defects.

Fig.9.deposition at different parameter

Pilot tests as shown in fig.9 was conducted at different parameters to obtain optimized process parameters. By changing the parameters, several single and multi-layer tracks were deposited. The final settings used for bulk CoCrNi-MEA deposition were those that produced a smooth single track and acceptable inter-layer bonding. The final optimized parameters are shown in the Table.1 below.

Table 1 Optimized parameters for experiments

Parameters	**Values**
Base plate material	Mild steel
Base plate dimension	150*
Work Material	(1) Ni-Cr alloy Wire (2) Co Wire
Wire diameter	1.2 mm
Voltage	14.5 V
Current	100A
Torch travel speed	125mm/min
Argon flow rate	20 l/min

4.5 Fabrication of CoCrNi-MEA using TWAAM:

By using Optimized process parameters CoCrNi-MEA a wall structure (108 * 10 * 24 mm) and a plate structure with 30% bead overlap (108 * 24 *6 mm) were deposited on a mild steel substrate plate.

(a) (b)

(c) (d)

(e) (f)

Fig .10. (a)(b)(e) Deposited. overlapping beads (30%) plate structures (c)(d)(f) Deposited Wall Structure

CHAPTER 5: NUMERICAL MODELLING AND SIMULATION

5.1 Transient thermo-mechanical modelling of TWAAM:

In order to determine residual stresses, a 3D transient thermal analysis is first carried out. The temperature output database is then entered into the structural model using plastic-elastic material behaviour.

The thermo-mechanical simulation is performed sequentially in two stages:

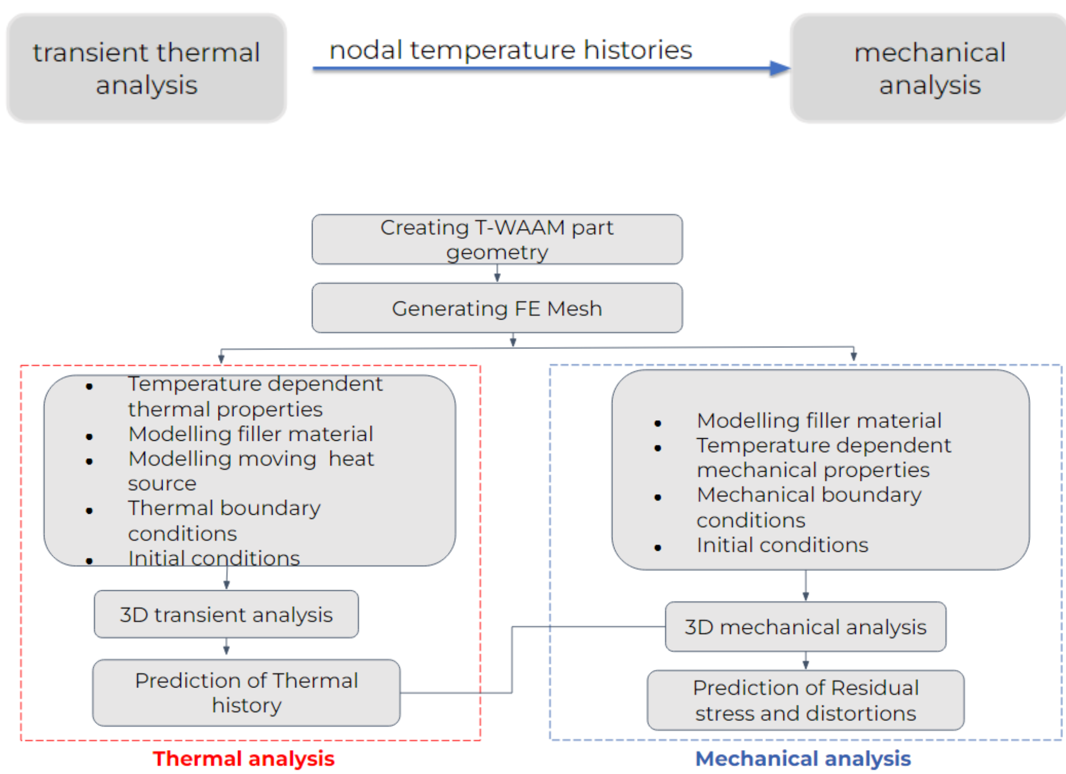

Fig. 11. Methodology of simulation

Key modelling aspects of Transient Thermo-Mechanical Analysis are:

(1) Heat source model

(2) Filler material model

(3) Material Properties

(4) Boundary conditions

5.2 Modelling of Heat source:

Heat source model is used to mimic the movement and physical phenomenon of arc generated which is utilized for melting the feedstock. During the TWAAM deposition we have two wire feedstocks merging into a single weld pool.

By superimposing two double-ellipsoidal heat sources separated by a distance or integrating the two heat sources into an equivalent Goldak heat source, the Goldak double-ellipsoidal heat source model, which is extensively used for moving heat sources, can be further extended to twin wire.[21]

Due to close proximity of two wires during twin-wire metal inert gas welding application, they associate with a single weld pool and they can be considered as a single elongated heat source [22]

The Goldak heat source is a double ellipsoidal heat source. It is combination of two different semi-ellipsoidal heat source volumes.[17]

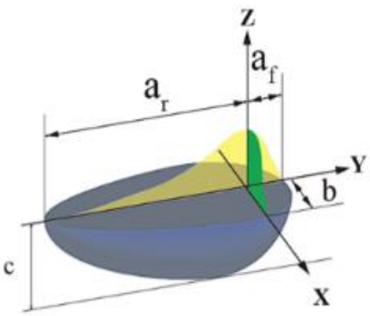

Fig. 12. Goldak Heat source model[22]

Power distribution in frontal ellipsoidal:

$$q_f(x,y,z,t) = \frac{6\sqrt{3}f_f Q}{a_f bc\pi\sqrt{\pi}} e^{\left(-\frac{3x^2}{a_f^2}\right)} e^{\left(\frac{-3[y-vt-y_0]^2}{b^2}\right)} e^{\left(-\frac{3z^2}{c^2}\right)} \ldots\ldots\ldots\ldots\ldots\ldots y \geq 0$$

Power distribution in rear ellipsoidal:

$$q_r(x,y,z,t) = \frac{6\sqrt{3}f_f Q}{a_r bc\pi\sqrt{\pi}} e^{\left(-\frac{3x^2}{a_r^2}\right)} e^{\left(\frac{-3[y-vt-y_0]^2}{b^2}\right)} e^{\left(-\frac{3z^2}{c^2}\right)} \ldots\ldots\ldots\ldots\ldots\ldots y < 0$$

$$\frac{f_f}{a_f} = \frac{f_r}{a_r}$$

$$f_f + f_r = 2$$

Where,

x, y, z are coordinates in the reference system

q_f,q_r (W/m^3) -power distribution in the front, and rear ellipsoids respectively.

efficiency (η)- assumed to be 0.85. The parameters, af ,ar , b, c is Goldak's molten pool characteristics. They are initially derived from weld pool ripple marks and optical macrograph of the deposited bead, transverse cross-section as in Fig. 13.

$a_f -$ front arc length,

a_r −rear arc length

b =half of the deposited bead width

c=sum of average of bead height and depth of penetration measured from bead

f_f, f_r-dimensionless fractions of the heat deposited in the front and rear half

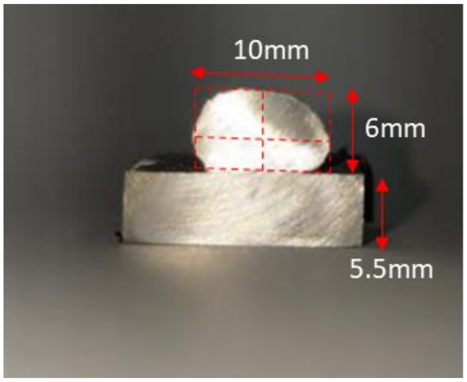

Fig.13. Bead Geometry used for modelling heat source model

Table 2 Calculated parameters used in the Goldak's heat source model

Parameter	Value
Length of front ellipsoidal (a_f) (mm)	3.6
Length of rear ellipsoidal (a_r) (mm)	14.4
Depth of the heat source (c) (mm)	6
Half width of the heat source (b) (mm)	5
Front heat fraction	0.4
Rear heat fraction	1.6
Energy input rate (W)	1450
Torch Speed(mm/min)	125

5.3 Modelling of Filler material:

The two most popular methods for simulating material deposition in the AM process are:

(1) Quiet Element Technique
(2) Element Birth Technique

All of the deposition's elements are constantly present during the analysis when using the quiet element technique. With the use of fictional material attributes that have no bearing on the simulation, all of the deposition's elements are rendered passive during the analysis phase of the quiet element technique. When the heat source gets close to the elements, the elements are given their actual properties.

Whereas,

In Element Birth Technique All the elements of the deposition track are deactivated in the initial step of the analysis and as the analysis proceeds, those elements are activated step by step.

Element Birth technique is widely used because of its computationally efficient.

5.4 Material Properties:

Commonly used Thermo-Mechanical Properties for simulations are Specific heat(J/Kg°C), Thermal conductivity(W/m°C), Density (Kg/m^3), Yield stress (MPa), Thermal expansion coefficient (10-5 /°C), Young Modulus (GPa) and Poisson's ratio.

CoCrNi-MEA is not been investigated enough and all the above-mentioned temperature dependent thermo-mechanical properties were not available in literature.

X.K. Zhu et all [23] investigated effects of temperature-dependent material properties on welding simulation. They concluded that Thermal conductivity has the most effect on the distribution of transient temperature field during welding. For the mechanical performance, yield stress has the most significant effect on the residual stress and distortion.

Based on literature we can say that when comprehensive temperature-dependent data are unavailable, it is advised to use material properties at room temperature, with the exception of the yield stress. [23]

Table 3 Temperature Dependent Properties of CoCrNi-MEA [24][25][26]

Temp	Thermal Conductivity	Density	Specific heat	Latent Heat	solidus Temp	Liquidous temp	Thermal Expansion coefficient alpha	Yield Stresses		Youngs modulus	poison ratio
K	k (W/(m·K))	(kg/m 3)	(J/(kg·K))	(J/kg)	K	K	K^{-1}	MPa		Pa	
300	28.67	8170	340	29,800	1323	1488	1.5e-5 at 673 K	77	340	2.35e11	0.31
400	31.3	8140	350					293	150		
600	35.42	8070	380					473	80		
800	38.91	7990	400					673	50		
1000	42.8	7900	420					873	5		
1200	44.78	7800	500								
1400	45	7620	840								
1600	47.36	7440	660								

Table 4 Temperature Dependent Properties of Substrate Plate –Mild Steel [27][28]

Temp	Thermal Conductivity	Density	Specific heat	Latent Heat	solidus Temp	Liquidous temp	Thermal Expansion coefficient alpha		Yield Stresses		Youngs modulus		poison ratio	
K	k (W/(m·K))	(kg/m 3)	(J/(kg·K))	(J/kg)	K	K	K^{-1}		MPa		Pa			
273.15	51.9	7860 Kg.m-3	486	2,70,000	1,723.2K	1,773.2K	293.15	1.17e-5	293.15	344.64 Mpa	293.15	2.06e11	293.15	0.296
373.15	51.1		486				373.15	1.17e-5	373.15	331.93	373.15	2.03e11	373.15	0.311
473.15	48.6		498				473.15	1.22e-5	473.15	308.3	473.15	2.01e11	473.15	0.33
573.15	44.4		515				573.15	1.28e-5	573.15	276.07	573.15	2e11	573.15	0.349
673.15	42.7		536				673.15	1.33e-5	673.15	235.22	673.15	1.65e11	673.15	0.367
773.15	39.4		557				773.15	1.38e-5	773.15	185.77	773.15	1e11	773.15	0.386
873.15	35.6		586				873.15	1.44e-5	873.15	127.71	873.15	6e11	873.15	0.405
973.15	31.8		619				973.15	1.48e-5	973.15	68.55	973.15	4e11	973.15	0.423
							1073.15	1.48e-5	1073.15	64.35	1073.15	3e11	1073.15	0.442
							1273.15	1.48e-5	1273.15	11.32	1273.15	1e11	1273.15	0.48
							3273.15	1.48e-5	3273.15		3273.15	1e11	3273.15	0.48

5.5 Boundary conditions:

The source of the elastic and plastic stresses that result in the ultimate residual stress state in the structure after welding is the transient temperature distribution. The energy is transferred from the heated weld to the boundaries through diffusion, i.e. through conduction in the material. Different conditions at the boundaries affects the heat transfer and temperature distribution. Also, similarly the mechanical constraints effect the cooling and heating leading to development of stress.

5.5.1 Thermal Boundary Condition

Convection and radiation heat loss are the primary boundary conditions that must be taken into account in the thermal analysis.

Newton's law of cooling is used for surface convection heat loss

$q_{conv} = h_{conv} (T - T_0)$

Where,

h_{conv} is convection heat transfer coefficient,

T_0 is ambient temperature

Stefan-Boltzmann's law for radiation heat loss are considered

$q_{rad} = \varepsilon.\ \sigma.\ ((T - T_Z)^4) - ((T_0 - T_Z)^4)$

Where,

ε is emissivity constant;

σ is Stefan-Boltzmann constant;

T_Z is Absolute zero on the actual temperature scale.

5.5.2 Mechanical Boundary Condition

For the mechanical analysis, the boundary conditions were carefully defined to accurately simulate the physical constraints of the TWAAM process. The substrate plate was constrained at all four corners to represent the fixture points used during the actual manufacturing process. Additionally, the constraints of the backing plate were also considered to ensure realistic simulation of the support structure's influence on the residual stresses.

5.6 Thermo-Mechanical modelling on ABAQUS:

Each module in ABAQUS/CAE defines a logical step in the modelling process, such as establishing the geometry, specifying the properties of the materials, and creating a mesh. Each module is used for specific purpose and then the complete model is developed. The model is then submitted in ABAQUS/CAE then generates an input file that is send to the ABAQUS analysis product after the model is finished. The input file created by ABAQUS/CAE is read by ABAQUS/Standard or ABAQUS/Explicit, which then does the analysis, provides data to ABAQUS/CAE so that job's progress can be tracked, and creates an output database. In order to visualize the outcomes of the analysis, the output database is read using the Visualization module.

5.6.1 Part Module

This module is used to define the geometry of deposition. The base plate was of dimension 150*70*5.5 mm and two deposition patterns were extruded. A wall structure of 108*10*24 lbh adna plate structure of 108*24*6mm was exruded on the base plate.

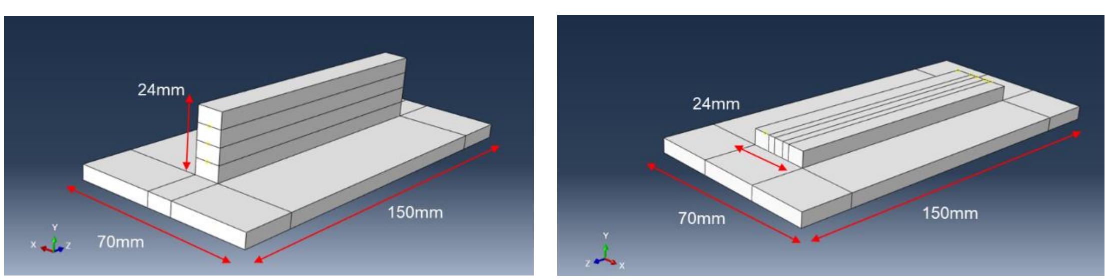

Fig. 14. Part geometry for deposition

5.6.2 Property Module:

The temperature-dependent thermo-mechanical material properties that will be employed in the study are defined in this module. Base plate is Mild Steel and the deposition is CoCrNi. Two different sections were made and predefined model was assigned.

5.6.3 Assembly Module:

The assembly is created and modified using the assembly module. There is just one assembly in the model, and it is made up of instances of the model's parts.

5.6.4 Step Module:

For Thermo-mechanical analysis we defined a heat transfer step for thermal analysis and static-general step for mechanical analysis.

5.6.5 Interaction Module:

This module is used to define the interaction in the simulation. Multiple interactions can be created for a single step. For modelling the filler material using element birth technique 'Model Change' interaction is used to activate and deactivate the elements at various steps. At Pre-Step it is used to deactivate all the element within the deposition geometry. Sequentially, all elements were then activated at suitable time step using the same interaction. Thermal boundary condition of convection and radiation interaction are also introduced at 'Pre-Step' step. For convection boundary condition a Film coefficient of 5.7 $\frac{w}{m^2k}$ and for radiation boundary condition emissivity of $\frac{w}{m^2k^4}$ were used.

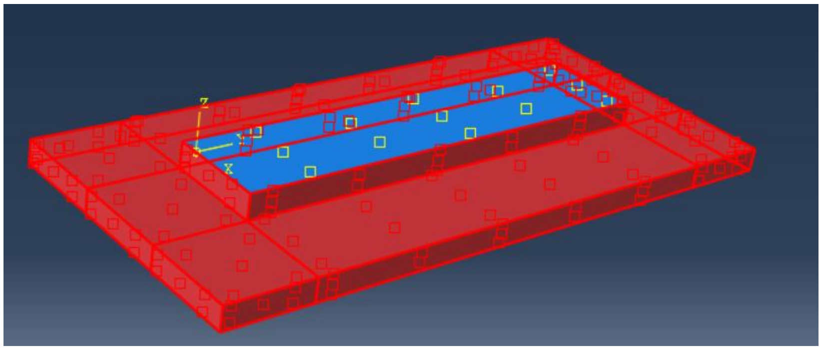

Fig. 15. Thermal boundary condition surfaces

5.6.6 Load Module:

This module is used to define the load at various steps.). For thermal analysis the heat source model is introduced using load module. In load module ‘Body Heat Flux’ was used and further ‘User-defined’ (since Goldak heat source model has user defined parameters) was selected. A DFLUX subroutine written in FORTRAN which has Goldak heat source model parameters coded.

In the mechanical analysis we don’t have any external load, the thermal field generated during the thermal analysis is introduced as the ‘Predefined Field’ which is also present in the load module.

5.6.7 Mesh Module :

Meshing of the generated part geometry is done using this module. Fine meshing is done near the deposition and courser meshing is done in rest of the region in order to reduce computational time. The mesh size was kept 1mm.

For the thermal analysis, a linear eight noded brick element (DC3D8) is utilized, and for the mechanical analysis, a linear eight noded brick element with reduced integration (C3D8R) with hour-glass control.

5.6.8 Job Module:

The job module is used to submit the job. The progress of the job and any error or warning can be seen in the window displayed on the job module.

5.6.9 Visualization Module:

Visualization module is used to do the analysis of the simulations are display through this module. The compiled ODB file is executed through this module.

5.7 Execution of thermo-mechanical transient model:

The thermal analysis was initially performed utilizing Abaqus modules. Heat input simulation was based on the Goldak heat source model, which was defined using a Fortran-written Dflux subroutine. Material deposition was conducted layer-by-layer through activating and deactivating interactions. The steps, interactions, and loads for this deposition process were generated using Python scripts. These scripts were then integrated with the ABAQUS 6.13 software and the DFLUX subroutine to conduct the analysis. The resulting data included the distribution of temperature and heat flux

Subsequently, a mechanical analysis was carried out using the temperature distribution obtained from the thermal analysis as a pre-defined field input. The resulting data included the distribution of residual stresses.

CHAPTER 6: RESULTS AND DISCUSSION

6.1 Results of thermal analysis:

Table 5 Nodal temperature distribution

<table>
<tr><td>Room Temperature</td><td>Preheated (300°C)</td></tr>
<tr><td>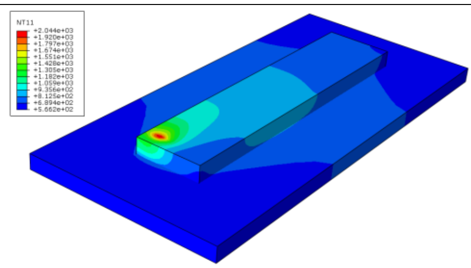</td><td>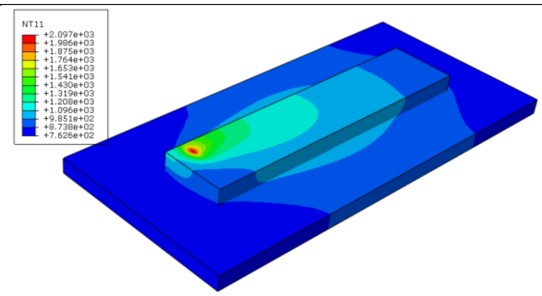</td></tr>
<tr><td>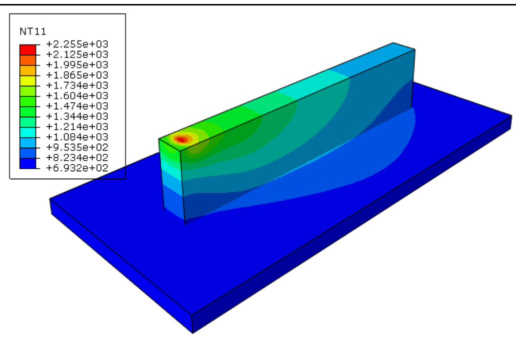</td><td>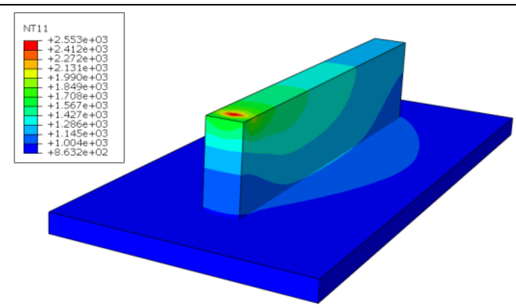</td></tr>
</table>

Table 6 Temperature distribution plots

<table>
<tr><th>s.no</th><th>Room Temperature</th><th>Preheated (300°C)</th></tr>
<tr><td>1</td><td>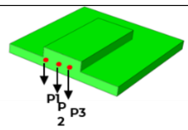

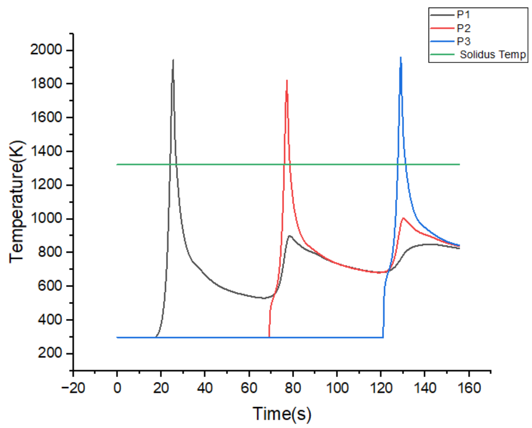
</td><td>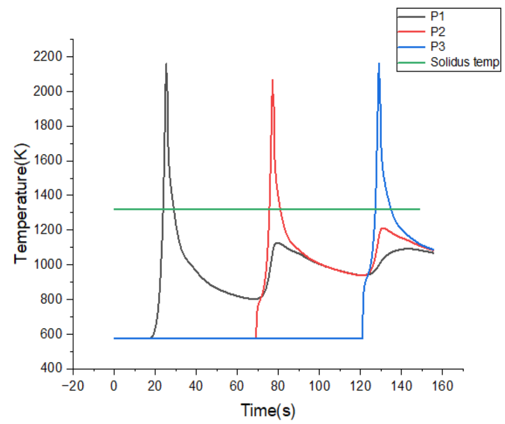
</td></tr>
<tr><td>2</td><td>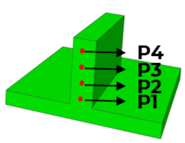

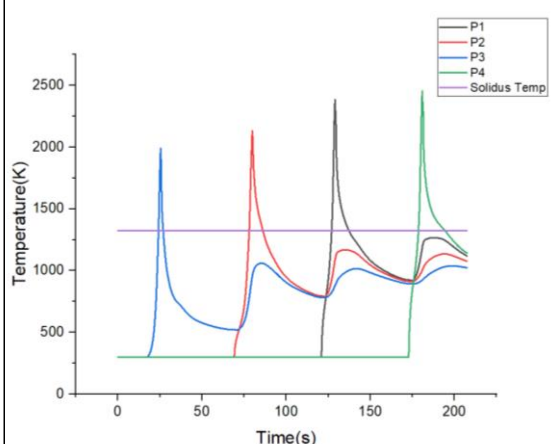
</td><td>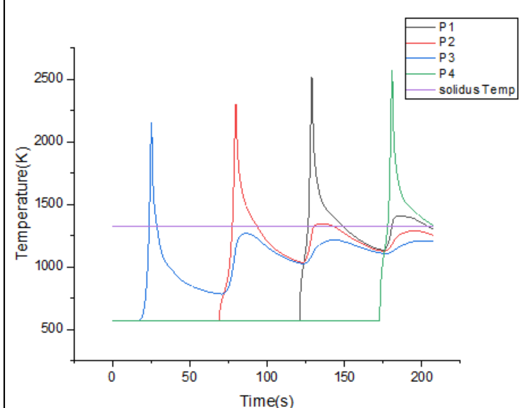
</td></tr>
</table>

The temperature distribution plot illustrates the temperatures at specific points over the deposition time. For the plate structure at room temperature, points 1 and 2 do not reach the solidus temperature during the second and third passes, indicating insufficient fusion between the layers. Even the temperature distribution in the preheated plate shows that the points do not reach the solidus temperature line, suggesting that preheating does not significantly enhance layer fusion in the plate structure.

For the block structure at room temperature, points 1, 2, and 3 do not reach the solidus temperature. However, with substrate preheating, point 1 almost reaches the solidus line during the second pass, while points 2 and 3 reach the solidus temperature in the second and third passes, respectively, indicating good fusion between the layers.

6.2 Results of Mechanical analysis:

Table 7 Residual Stress Distribution

S.no	Structure	Stress Distribution
1	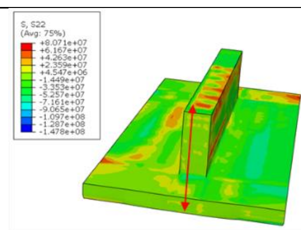	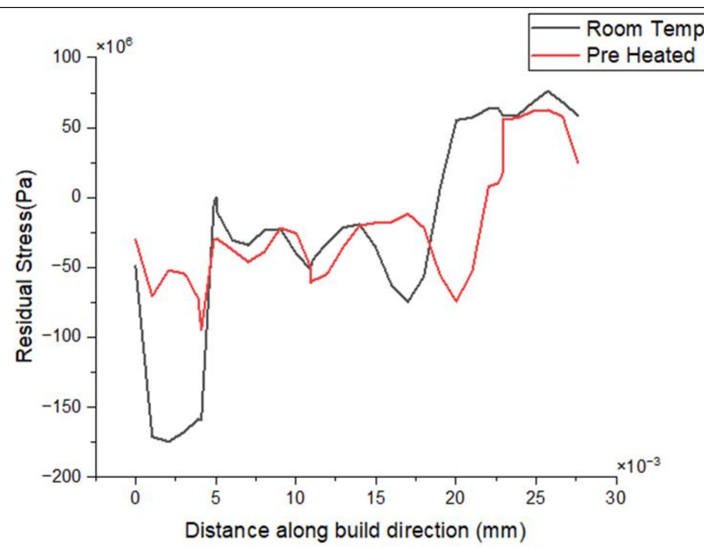

2	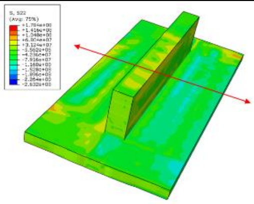	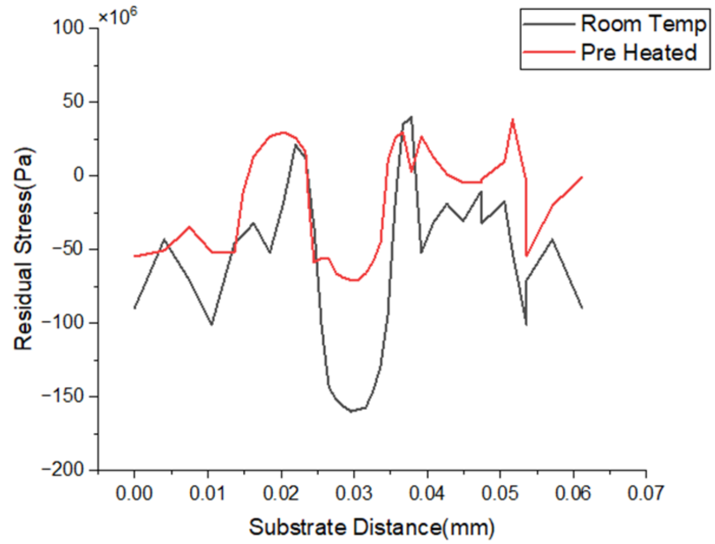
3	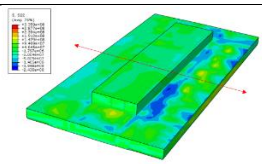	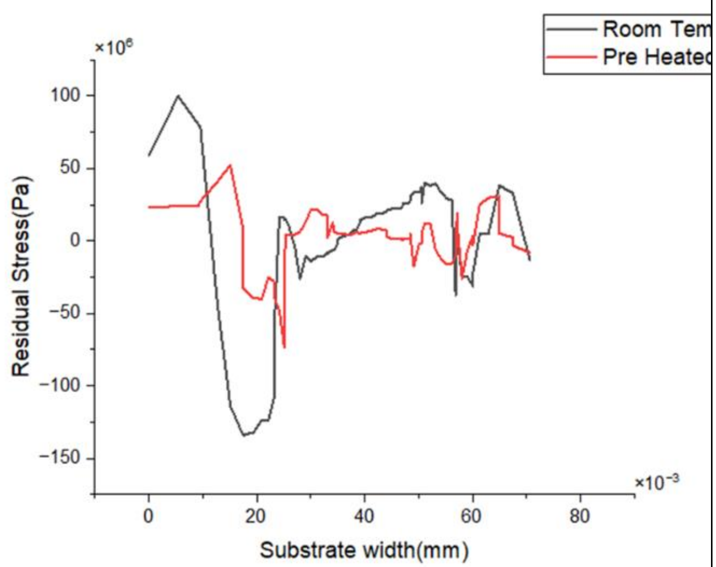

The residual stress distribution for wall structure across the substrate and build geometry along the Z-direction (Table 7 s.no 1) shows that while the substrate plate experiences compressive stresses, the stresses transition to tensile as we move towards the top layer. At room temperature, the maximum and minimum stresses observed were -159.6 MPa (compressive) and +62.1 MPa (tensile), respectively. After preheating, these stresses were mitigated, with the maximum stress reduced to -70.8 MPa (compressive) and the minimum stress reduced to +52.2 MPa (tensile). Substrate preheating significantly reduces residual stress within the substrate. However, this effect diminishes as we move further from the substrate, indicating a localized impact of preheating on residual stress reduction.

The residual stress distribution for wall structure across the substrate plate along the X direction (Table 7, s.no 2) indicates high compressive stresses near the deposition zone. At room temperature, the maximum and minimum stresses observed were -174.6 MPa (compressive) and +63.5 MPa (tensile), respectively. After preheating, these stresses were mitigated, with the maximum stress reduced to -94.7 MPa (compressive) and the minimum stress reduced to +62.4 MPa (tensile). Substrate preheating significantly reduces these compressive stresses by mitigating the thermal gradient and allowing more uniform expansion and contraction, thereby reducing the overall stress distribution.

The residual stress distribution for the plate structure across the substrate plate along the X direction (Table 7 s.no 3) indicates that during the first pass, the substrate experiences high compressive stresses. At room temperature, the maximum and minimum stresses observed were -134.0 (compressive) and +99.9 MPa (tensile), respectively. After preheating, these stresses were mitigated, with the maximum stress reduced to -73.4 MPa (compressive) and the minimum stress reduced to +52.3MPa (tensile). This initial buildup of compressive stresses is characteristic of the welding process, as rapid heating and cooling induce thermal gradients, resulting in constrained shrinkage and stress accumulation. However, as the welding progresses, the thermal effects become more balanced, leading to a reduction in compressive stresses in the substrate. Moreover, preheating the substrate plate exhibits a significant reduction in compressive stresses, particularly during the first pass.

6.3 Experimental Residual stress Analysis:

4 samples were scanned, two from each deposition. 1 sample was cut out from the substrate and the other one from the deposition top layer. Sample requirement for XRD were Min 10*10mm and maximum 12mm thick. Substrate were cut through 20*20*5.5 and deposition 20*20*10

Measurement and Analysis Using XRD

X-ray diffraction (XRD) can be used to measure the residual stresses by analysing the d-spacing variations at different tilt angles (ψ). Here's a step-by-step method to assess the residual stress distribution:

1. **Sample Preparation**:
   - Cut cross-sectional samples from the wall structure, ensuring that sections from different heights and the interface are included.
2. **XRD Measurements**:
   - Perform XRD measurements at various points across the cross-section.
   - Measure the d-spacing at different ψ angles to determine the strain.
3. **Data Analysis**:
   - Plot d-spacing versus $\sin^2\psi$ and perform linear regression to find the slope (m) at each point.
4. **Residual Stress Calculation**:
   - Use the slope (m) to calculate the residual stress (σ) at each point using the formula[29] :

$$\boldsymbol{\sigma = \frac{mE}{(1+\nu)d_0}}$$

Where,

σ -Residual stress

d_0 -Lattice spacing

E -Young's modulus

ν-Poisson's ratio

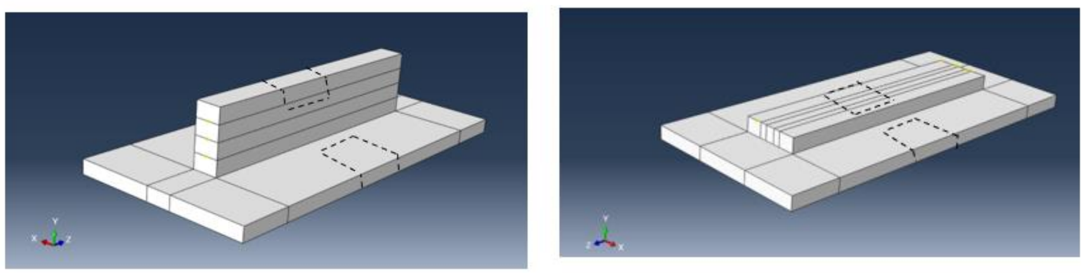

Fig. 16. Sample cutout geometry

Table 8 Calculated Residual Stresses

1	Wall build substrate(Mild Steel)	-989.27 MPa
2	Wall build deposit(CoCrNi-MEA)	-4300MPa
3	Plate deposit (CoCrNi-MEA)	704.49MPa
4	Plate substrate (Mild Steel)	-537.1MPa

CHAPTER 7: CONCLUSIONS AND FUTURE SCOPE

Conclusions

- Experimental fabrication of CoCrNi wall and plate structures using optimized parameters demonstrated the feasibility of TWAAM for MEA.

- The development of a numerical simulation model provided a comprehensive understanding of the TWAAM process, facilitating the prediction and analysis of temperature distribution and residual stresses in fabricated components.

- Preheating of Substrate Plate helps in better fusion of upcoming layers with the existing layer. It also significantly reduces the residual stress

Future scope of work

- Thermal cycle can be experimentally validated by using online temperature monitoring tools and using temperature sensor.
- The presented simulation model can be fully automated with the help of python codes, which would eventually parameters.
- Investigation of mechanical properties and microstructural characterization of deposited CoCrNi-MEA structures
- Comparative study of mechanical properties of CoCrNi- MEA fabricated by different print patterns
- Micro-scale modelling of T-WAAM can provide deep insights into the material properties, defect formation, and microstructural characteristics.

CHAPTER 8: REFERENCES

1. https://www.symmetryelectronics.com/blog/defining-additive-manufacturing/
2. Chaturvedi, Mukti, et al. "Wire arc additive manufacturing: Review on recent findings and challenges in industrial applications and materials characterization." Metals 11.6 (2021): 939
3. Li, Yan, Chen Su, and Jianjun Zhu. "Comprehensive review of wire arc additive manufacturing: Hardware system, physical process, monitoring, property characterization, application and future prospects." Results in Engineering 13(2022):100330.
4. Baby, Justin, and Murugaiyan Amirthalingam. "Microstructural development during wire arc additive manufacturing of copper-based components." Welding in the World 64.2(2020): 395-405.
5. Deshmukh, Poonam S., and Dan Sathiaraj. "A Review on Twin Wire Arc Additive Manufacturing of Metals and Alloys: Microstructure and Mechanical Properties." Recent Advances in Manufacturing Processes and Systems: Select Proceedings of RAM 2021 (2022): 55-67.
6. Zhang, Meng, et al. "Microstructure and mechanical properties of twin wire and arc additive manufactured Ni3Al-based alloy." Journal of Materials Processing Technology 303 (2022): 117529
7. Deshmukh, Poonam S., et al. "Nano to macro-mechanical properties of laser directed energy deposited CoCrNi medium entropy alloy." Materials Today Communications 35(2023): 106351.
8. He, Hua, et al. "Review on the preparation methods and strengthening mechanisms of medium-entropy alloys with CoCrNi as the main focus." Journal of Materials Research and Technology 27 (2023): 6275-6307.
9. Chen, Shu-guang, et al. "Review on residual stresses in metal additive manufacturing:formation mechanisms, parameter dependencies, prediction and control approaches." Journal of materials research and technology 17 (2022): 2950-2974.

10. . Montevecchi, Filippo, et al. "Finite element modelling of wire-arc-additive-manufacturing process." Procedia Cirp 55 (2016): 109-114.
11. . Weng, Fei, et al. "Excellent combination of strength and ductility of CoCrNi medium entropy alloy fabricated by laser aided additive manufacturing." Additive Manufacturing 34 (2020): 101202.
12. Jung, Kyung-Hwan, et al. "Correlation of cryogenic deformation mechanisms to excellent strength-ductility of CrCoNi medium entropy alloy processed by selective laser mmelting."Journal of Materials Research and Technology 22 (2023): 2297-2315.
13. Williams, Stewart W., et al. "Wire+ arc additive manufacturing." Materials science and technology 32.7 (2016): 641-647.
14. Saadatmand, Mohsen, and Reza Talemi. "Study on the thermal cycle of Wire Arc Additive Manufactured (WAAM) carbon steel wall using numerical simulation." Fratturaed Integrità Strutturale 14.52 (2020): 98-104.
15. Somashekara, M. A., and S. Suryakumar. "Studies on dissimilar twin-wire weld-deposition for additive manufacturing applications." Transactions of the Indian Institute of Metals 70 (2017): 2123-2135.
16. Pramod, R., et al. "Fabrication of gas metal arc welding based wire plus arc additive manufactured 347 stainless steel structure: behavioral analysis through experimentation and finite element method." Metals and Materials International 28.1 (2022): 307-321.
17. . Goldak, J., Chakravarti, A. & Bibby, M. A new finite element model for welding heat sources. Metall Trans B 15, 299–305 (1984).
18. . Mishra, Rajnish, et al. "Experimental and numerical investigation of double pass overlapping beads by twin-wire welding additive manufacturing process." Transactions of the Indian Institute of Metals 76.2 (2023): 297-313.
19. Sun, Jiamin, et al. "Residual stress in wire and arc additively manufactured aluminum components." Journal of Manufacturing Processes 65 (2021): 97-111.

20. Mishra, Rajnish, et al. "Thermo-mechanical modelling of the wire arc based additively manufactured Inconel 625 superalloy." Materials Today: Proceedings (2023).
21. Mishra, R., Pillai, A., Imam, M. et al. Experimental and Numerical Investigation of Double Pass Overlapping Beads by Twin-Wire Welding Additive Manufacturing Process. Trans Indian Inst Met 76, 297–313 (2023).
22. . Sharma, A., Chaudhary, A.K., Arora, N. et al. Estimation of heat source modelparameters for twin-wire submerged arc welding. Int J Adv Manuf Technol 45, 1096(2009).
23. . Zhu, X. K., and Y. J. Chao. "Effects of temperature-dependent material properties on welding simulation." Computers & Structures 80.11 (2002): 967-976.
24. Jung, Kyung-Hwan, et al. "Correlation of cryogenic deformation mechanisms to Excellent strength-ductility of CrCoNi medium entropy alloy processed by selective laser melting."Journal of Materials Research and Technology 22 (2023): 2297-2315.
25. Laplanche, G., et al. "Elastic moduli and thermal expansion coefficients of medium-entropy subsystems of the CrMnFeCoNi high-entropy alloy." Journal of Alloys and Compounds 746 (2018): 244-255.
26. Schneider, M., et al. "Analysis of strengthening due to grain boundaries and annealing twin boundaries in the CrCoNi medium-entropy alloy." International Journal of Plasticity 124 (2020): 155-169.
27. Zhang, Lu, and P. Michaleris. "Investigation of Lagrangian and Eulerian finite element methods for modeling the laser forming process." Finite elements in analysis and design 40.4 (2004): 383-405.
28. . Belhadj, Mohamed, et al. "Thermal anal Thermal analysis of Wir sis of Wire Arc Additive Manufacturing pr acturing process."
29. Rathinasuriyan, C., and VS Senthil Kumar. "Experimental investigation of weld characteristics on submerged friction stir welded 6061-T6 aluminum alloy." Journal of Mechanical Science and Technology 31 (2017): 3925-3933.